# Impact of heat treatment process on threshold current density in AlGaN-based deep-ultraviolet laser diodes on AlN substrate

Maki Kushimoto[1]*, Ziyi Zhang[2,3], Naoharu Sugiyama[2], Yoshio Honda[2], Leo J. Schowalter[2,4], Chiaki Sasaoka[2], and Hiroshi Amano[2],

[1]*Graduate School of Engineering, Nagoya University, Furo-cho, Chikusa-ku, Aichi 464-8603, Japan*
[2]*Center for Integrated Research of Future Electronics, Institute of Materials Research and System for Sustainability, Nagoya University, Furo-cho, Chikusa-ku, Aichi 464-8601, Japan*
[3]*Innovative Devices R&D Center, Corporate Research & Development, Asahi Kasei Corporation, Fuji, Shizuoka 416-8501, Japan*
[4]*Crystal IS, 70 Cohoes Avenue, Green Island, NY 12183, U.S.A.*

The electroluminescence (EL) uniformity of AlGaN-based deep UV laser diodes on AlN substrate was analyzed by using the EL imaging technique. Although nonuniform EL patterns were observed, the uniformity was improved by changing the position of the p-electrode. The threshold current density was also reduced by suppressing the inhomogeneity of the EL. Cathodoluminescence analysis revealed that the cause of the non-uniformity is the degradation of the active layer and the nonuniformity emission formed by rapid thermal annealing at high temperature after mesa structure formation.

Laser diodes (LDs) operating in the UV wavelength range are promising as a low-cost, compact light source for various of applications such as sterilization, bio-/chemical analysis, medical treatment, and material processing.[1)] Development of short-wavelength LDs based on AlGaN materials has been pursued for years. Recently, room-temperature, pulsed lasing in UV-C[2,3)] and UV-B[4)] wavelength regions has been realized by improving the crystal quality of AlGaN and realizing a high hole concentration and low light absorption in the p-type cladding layer[5,6)] by utilizing distributed polarization doping.[7,8)] However, continuous wave lasing, which is desired for these devices to be practical, has not yet been achieved. The challenge is to reduce the high threshold current densities and operating voltage compared with those of other nitride laser diodes.[9)]

To achieve low-threshold deep UV LDs, the appropriate design of the stacked structure is essential,[10)] and crystal quality is also important. The appearance of crystal imperfections such as dislocations[11)] and/or point defects[12,13)] may cause low radiative recombination efficiency at

*E-mail: kushimoto@nuee.nagoya-u.ac.jp

active layers as well as high internal loss due to the absorption[14,15] and scattering of light.[16,17] To realize a low-dislocation AlGaN active layer, pseudomorphic crystal growth on a single-crystal AlN substrate with low dislocation is essential.[18,19] High radiative recombination efficiency was reported for the AlGaN active layer[20] and LEDs[21] grown on single-crystal AlN substrates. AlGaN-based optical cavities on single-crystal AlN substrates can also achieve significantly lower threshold power densities than those on heterogeneous substrates.[22–24] There have been many studies on the factors that degrade device characteristics caused by the epitaxial crystal growth; however, there is not much discussion on the degradation of AlGaN-based devices caused by device fabrication.

In this study, the electroluminescence imaging (ELI) technique[25] was used to identify nondestructively the macroscopic nonuniformity of emission from the active layer of the fabricated LD devices. This technique allows us to clarify the relationship between the device threshold current densities and the emission patterns. Cathodoluminescence (CL) analysis suggests that the thermal process in the current device fabrication is likely to cause defect formation in the vicinity of the mesa boundary, and those defects result in higher threshold current densities in the LD devices.

The AlGaN LD structure was grown by metal organic vapor phase epitaxy on single-crystal AlN substrates. The AlGaN-based active layer was sandwiched between the $Al_{0.63}Ga_{0.37}N$ guiding layer and the $Al_{0.7}Ga_{0.3}N$ cladding layer. The active layer consists of two quantum wells, and the thickness and Al composition of the well and barrier layers are 3 nm, 53%, and 6 nm, 63%, respectively. The p-type cladding layer was using distributed polarization doping techniques where the Al composition was varied from 1 to 0.7 in the growth direction. The p-contact layer itself was p-GaN. The detailed epistructure can be found in a previous report.[2] The device fabrication was carried out in the Center for Integrated Research of Future Electronics, Transformative Electronics Facilities (C-TEFs) of Nagoya University. The LD devices were fabricated as follows: p-activation annealing at 900 $^{o}$C, mesa and ridge structure formation by inductively coupled plasma dry etching to expose the n-contact layer and to construct current, deposition of $SiO_2$ passivation layer, V/Al/Ti/Au-based n-electrode formation, rapid thermal annealing (RTA) at 850 $^{o}$C for 2 min in nitrogen atmosphere, Ni/Au-based p-stripe electrode formation, RTA at 525 $^{o}$C in oxygen atmosphere, and pad electrode formation. For the formation of the ridge structure, etching was performed up to the middle of the DPD structure. The length of the gap between the p-electrode stripes and the mesa edges (p/mesa gap) was set to be 5, 10, or 15 $\mu$m. Then the wafers were thinned down and cleaved to form 400-$\mu$m-long LD bars. The sides of the cleaved facets of these LD bars were then

coated with five periods of $HfO_2/SiO_2$ to form highly reflective mirrors.

The laser bars firstly undergo L–I measurement with 2 kHz, 100 ns width pulsed current injection to determine the threshold current density. ELI was then performed under a DC current well below the threshold current. The LDs were mounted on a quartz plate and the luminescence pattern was observed from the back surface of the AlN substrate through the UV-transparent quartz plate. A UV-transparent and low-wavelength-dispersion objective lens with 10× magnification and a UV CCD camera were used for ELI. Neutral density filters and a 315 nm short-pass edge filter were used for light intensity control and chromatic aberration reduction, respectively. A detailed analysis of the CL emission patterns was performed on partially processed samples, prepared from the same wafers, where only the mesa structures were etched. To investigate the effect of thermal processing on the emission patterns, the samples were treated by RTA at a temperature of 400, 600, or 850 $^{o}$C after the 1st $SiO_2$ passivation. The RTA conditions were similar to those of the n-electrode formation except for the annealing temperature.

Figure 1 shows the measured threshold current density of the UV-C LDs. The lasing wavelength of the measured samples was 271.2 ± 0.8 nm. As the size of the p/mesa gap increased, the threshold current density decreased. Particularly for 5-$\mu$m-gap-width LDs, some of these devices were not lasing, which is not plotted on this figure. The length of the p/mesa gap was correlated with the luminescence inhomogeneity and threshold current density. This suggests that inhomogeneity luminescence leads to a higher threshold current density. The average series resistance of LDs with 5, 10, and 15 $\mu$m gap widths were 10, 13, and 17 Ω, respectively. This increase in resistance is due to the extension of the lateral flow path through the n-AlGaN region. Therefore, the change in gap length is a trade-off between the threshold current density and the resistance.

The EL images observed from the backside of the AlN substrate are shown in Fig. 2. The thin, bright line of luminescence to the right of the ridge is due to EL leaking from the mesa edge and, thus, definitively marks the mesa edge. There were no changes in the ELI patterns for the current densities up to 0.75 kA/cm$^2$. Linear and spotty dark regions are found in the EL image of LDs with a p/mesa gap of 5 $\mu$m. In addition, dark regions were also observed in the EL image of LDs with a 10 $\mu$m p/mesa gap; these dark regions are located on the right side of the light emitting area, close to the mesa edge. A linear dark line is approximately parallel to the a-axis direction. On the other hand, for the LDs with a 15 $\mu$m gap width, hardly any dark regions were observed. When the gap length was further increased, no dark areas were observed as well. Increasing the p/mesa gap was found to significantly improve

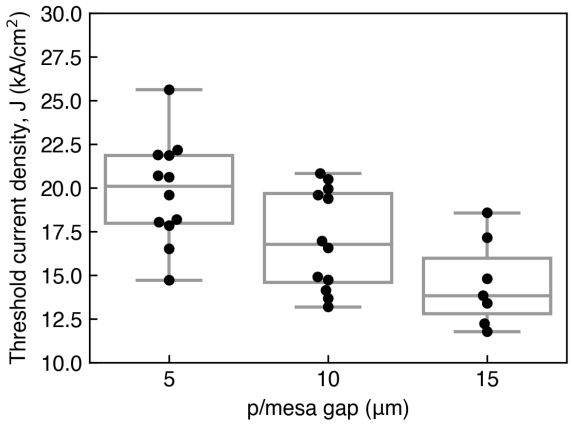


**Fig. 1.** Threshold current density of LDs with different gap widths.

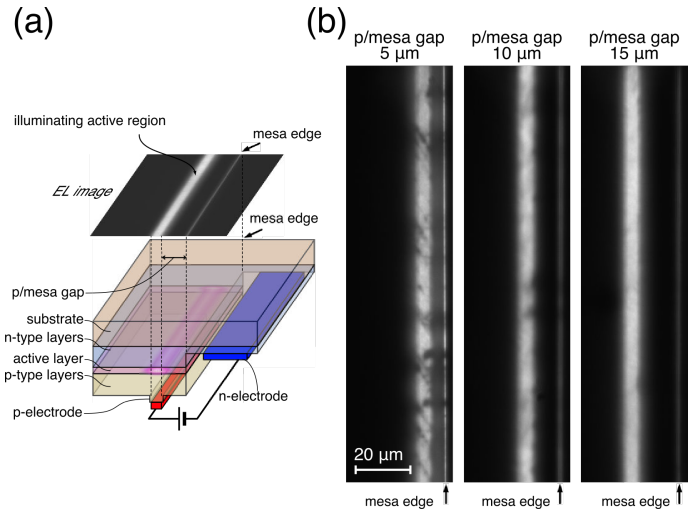


**Fig. 2.** (a) Schematic diagram of ELI measurement. (b) Optical microscopy images of the electroluminescence from the backside of the AlN substrate. LDs with p/mesa gap widths between 5 and 15 $\mu$m were driven at a current density of 0.75 kA/cm$^2$. Emission leaking from the mesa edge result in the thin, bright line seen to the right of the EL from the ridge region.

the luminescence uniformity under weak current injection. These nonuniformities suggest the presence of nonuniform emission from the active layer or nonuniform current injection into the active layer.

To investigate the cause of the EL emission nonuniformity, CL images were observed at room temperature. Figure 3(a) shows monochromatic CL and SEM images of the area near the mesa edge. The detection wavelength of the CL image was set to the emission wavelength from the active layer. In the CL image, a dark area was observed near the mesa edge, and the CL intensity decreases as it approaches the mesa edge. In this dark area, dark lines along the

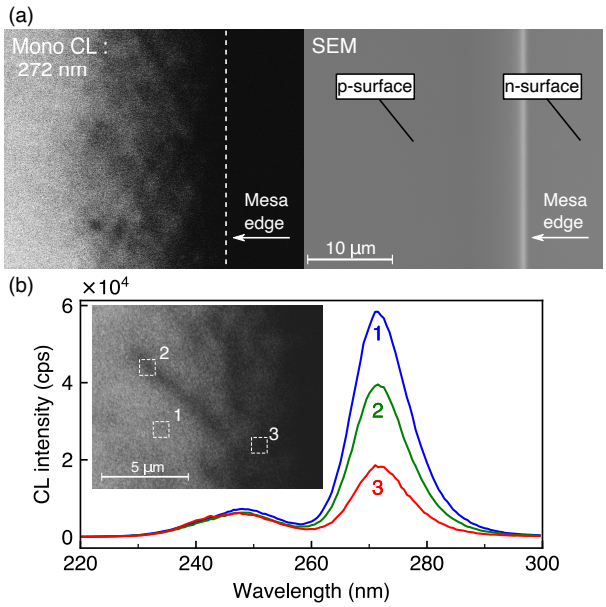


**Fig. 3.** (a) Monochromatic CL image and surface SEM image at the wavelength of 272 nm taken on the same area of the mesa edge. (b) Monochromatic CL images and CL spectra in the vicinity of the dark region formed on mesa. The three regions where the spectra were acquired are shown as dotted squares.

a-axis direction were also observed. This dark area disappeared within 15 $\mu$m from the mesa edge toward the center. Neither of these features were observed in the SEM image. Therefore, the formation of dark regions is not caused by an abnormal growth or other factors that change the surface morphology. Figure 3(b) shows the CL spectra observed in and around a dark region. The CL intensity was lower at positions 2 and 3 than at position 1. However, no peak wavelength shift was observed, and the relatively scaled emission spectra from active layer remained the same. This indicates that the dark region is caused by nonradiative recombination rather than by distortions of the structure or the composition of the active layer. The patterns of dark regions observed in the CL images are comparable to those of the dark regions that appear in the EL images. These dark regions were observed only in the vicinity of the mesa, suggesting that they were formed after mesa formation.

To investigate the formation mechanism of the dark regions, CL analysis was performed for samples that underwent mesa formation and RTA at various temperatures. Figure 4 shows monochromatic CL images from the active layer (measured at 272 nm) and n-AlGaN (measured at 242 nm) for each of the different processes. No explicit dark region appeared in the CL images over the whole mesa structure in the samples that either experienced no RTA or an RTA at 400 $^{o}$C. In the sample with the RTA temperature of 600 $^{o}$C, a dark region was formed over the entire region of about 2 $\mu$m from the mesa edge. As the RTA temperature

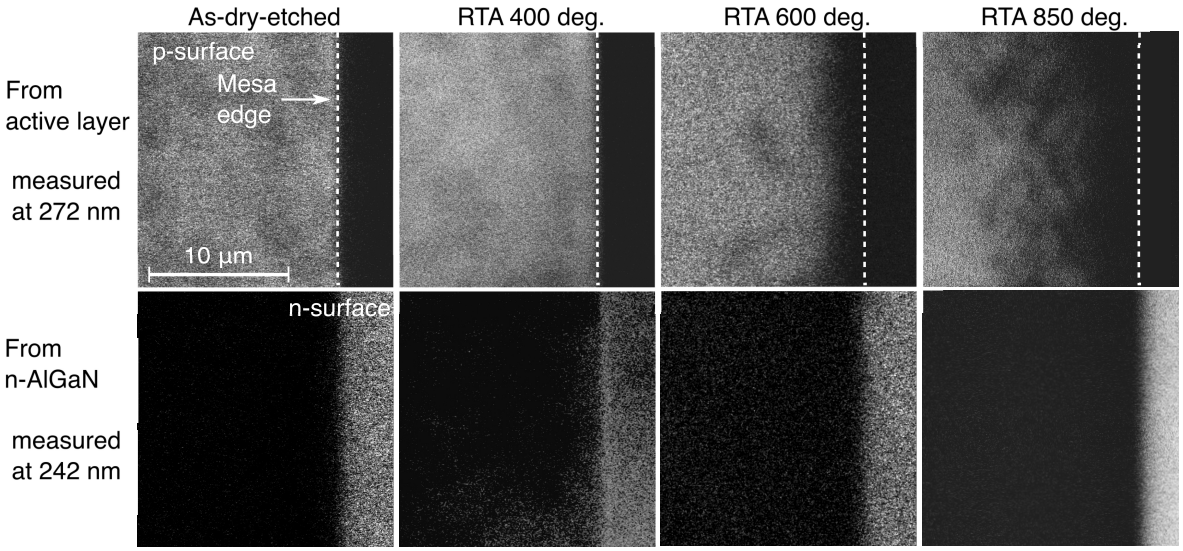


**Fig. 4.** Surface monochromatic CL images near the mesa edge at wavelengths of 272 and 242 nm. The former shows emission from the active layer and the latter from the n-$Al_{0.7}Ga_{0.3}N$ layer. The boundary of mesa structure is clearly indicated by the CL image of 242 nm emission, since the weaker excitation of n-AlGaN and absorbance of emission by existing p-sided layers at mesa region. The samples were dry-etched without annealing and dry-etched with RTA at 400, 600 and 850 $^{o}$C in nitrogen ambient.

was increased to 850 $^{o}$C, the dark region near the mesa edge extended to the mesa region and dark lines appeared.

The experimental results show that weakly radiative recombination regions, which appeared as dark lines/spots in the EL and CL images, are formed near the mesa edge. Since the distribution of these dark regions was limited to areas relatively close to the mesa edge, nonuniform emission (and the resultant increase in the threshold current density) can be suppressed by widening the p/mesa gap. These dark regions were formed by high-temperature annealing. Thus, the nonuniformity of EL emission was not due to the nonuniformity of current injection, as observed in the degradation of InGaN LDs,[26] but was rather due to the defects introduced in the active layer by the mesa etching and thermal processing. Taking account of the fact that the LD structures were grown pseudomorphically on a single-crystal AlN substrate with dislocation densities less than $10^4$ cm$^{-2}$, and that the dark areas only appeared near the mesa edge, the cause of these dark areas must be defects unrelated to threading dislocations from the substrate or epitaxial growth process. It is found that dislocations are exist within the active layer of 850 $^{o}$C annealed samples by a preliminary cross sectional TEM measurement. The region where the dislocation exists roughly matched where the net-like dark lines in CL image appeared after annealing. Meanwhile, in the CL image, the dark lines are denser toward

the edge of the mesa, which cannot be explained by the distribution of dislocations found in the TEM observation. Therefore, the overall dark region formation in the vicinity of the mesa edge may be partly attributed to dislocation formation, it seems that there are other causes. The net-like dark lines that appeared in the CL images are similar to what has been observed in semipolar GaN[27,28] and InGaN on GaN with low dislocation density.[29–31] Since these dislocations are introduced to relieve stress in InGaN/GaN through the slip plane, it is possible that the dislocations in this study were also formed to relieve stress. The details of these dislocation should be clarified by structural analysis. On the other hand, no dislocation was observed in the active layer at the mesa edge, suggesting the possibility of point defects. InGaAs and InP-based LDs, point defects are induced during dry etching to form ridges, and that the point defects diffuse during heat treatment,[32] resulting in nonradiative recombination at the edges of the ridges.[33] Even in GaN, it has been reported that dry etching causes damage to the etched surface.[34] Since the migration barrier of the native defect in GaN is relatively small and Ga vacancies are formed by electron irradiation and diffuse at temperatures below 600 K,[35,36] which may be the cause of the dark areas spreading during annealing at 600 °C or higher in the AlGaN layers used for these LDs.

In conclusion, it was found that the non-uniformity of the EL emission characteristics of UV-C LDs depends on the arrangement of the p-electrode. Particularly, when the p-electrode was placed near the mesa edge, the threshold current density of the UV-C LDs was found to increase significantly. CL observations revealed that the EL non-uniformity at the mesa edge, which is the cause of the deterioration of LD characteristics, is caused by the high temperature annealing at 600 °C or higher. The results of this study suggest that the considering of the active layer degradation near the mesa edge due to the annealing process in UV-C LDs is extremely important in the structural and process design to reduce the threshold current density.

**Acknowledgment**

The authors would like to thank Professor Nobuyuki Ikarashi of Nagoya University, Mr. Kazuhiro Nagase and Dr. Naohiro Kuze of Asahi Kasei Corporation for their invaluable discussion and considerable support.

## References


1) M. Kneissl, T.Y. Seong, J. Han, and H. Amano, Nat. Photonics **13**, 233 (2019).
2) Z. Zhang, M. Kushimoto, T. Sakai, N. Sugiyama, L.J. Schowalter, C. Sasaoka, and H. Amano, Appl. Phys. Express **12**, 124003 (2019).
3) T. Sakai, M. Kushimoto, Z. Zhang, N. Sugiyama, L.J. Schowalter, Y. Honda, C. Sasaoka, and H. Amano, Appl. Phys. Lett. **116**, 122101 (2020).
4) K. Sato, S. Yasue, K. Yamada, S. Tanaka, T. Omori, S. Ishizuka, S. Teramura, Y. Ogino, S. Iwayama, H. Miyake, M. Iwaya, T. Takeuchi, S. Kamiyama, and I. Akasaki, Appl. Phys. Express **13**, 031004 (2020).
5) Z. Zhang, M. Kushimoto, M. Horita, N. Sugiyama, L.J. Schowalter, C. Sasaoka, and H. Amano, Appl. Phys. Lett. **117**, 152104 (2020).
6) Z. Zhang, M. Kushimoto, T. Sakai, N. Sugiyama, L.J. Schowalter, C. Sasaoka, and H. Amano, Jpn. J. Appl. Phys. **59**, 094001 (2020).
7) D. Jena, S. Heikman, D. Green, D. Buttari, R. Coffie, H. Xing, S. Keller, S. DenBaars, J.S. Speck, U.K. Mishra, and I. Smorchkova, Appl. Phys. Lett. **81**, 4395 (2002).
8) J. Simon, V. Protasenko, C. Lian, H. Xing, and D. Jena, Science **327**, 60 (2010).
9) H. Amano, R. Collazo, C. De Santi, S. Einfeldt, M. Funato, J. Glaab, S. Hagedorn, A. Hirano, H. Hirayama, R. Ishii, Y. Kashima, Y. Kawakami, R. Kirste, M. Kneissl, R. Martin, F. Mehnke, M. Meneghini, A. Ougazzaden, P.J. Parbrook, S. Rajan, P. Reddy, F. Römer, J. Ruschel, B. Sarkar, F. Scholz, L.J. Schowalter, P. Shields, Z. Sitar, L. Sulmoni, T. Wang, T. Wernicke, M. Weyers, B. Witzigmann, Y.-R. Wu, T. Wunderer, and Y. Zhang, J. Phys. D. Appl. Phys. **53**, 503001 (2020).
10) W.W. Chow, M. Kneissl, J.E. Northrup, and N.M. Johnson, Appl. Phys. Lett. **90**, 101116 (2007).
11) K. Ban, J. Yamamoto, K. Takeda, K. Ide, M. Iwaya, T. Takeuchi, S. Kamiyama, I. Akasaki, and H. Amano, Appl. Phys. Express **4**, 052101 (2011).
12) A. Armstrong, A.A. Allerman, T.A. Henry, and M.H. Crawford, Appl. Phys. Lett. **98**, 10 (2011).
13) H. Murotani, D. Akase, K. Anai, Y. Yamada, H. Miyake, and K. Hiramatsu, Appl. Phys. Lett. **101**, 042110 (2012).
14) W.C. Ke, C.S. Ku, H.Y. Huang, W.C. Chen, L. Lee, W.K. Chen, W.C. Chou, W.H. Chen, M.C. Lee, W.J. Lin, Y.C. Cheng, and Y.T. Cherng, Appl. Phys. Lett. **85**, 3047 (2004).
15) H. Hasegawa, Y. Kamimura, K. Edagawa, and I. Yonenaga, J. Appl. Phys. **102**, 2005

(2007).

16) N.G. Weimann, L.F. Eastman, D. Doppalapudi, H.M. Ng, and T.D. Moustakas, J. Appl. Phys. **83**, 3656 (1998).

17) C. Kuhn, M. Martens, F. Mehnke, J. Enslin, P. Schneider, C. Reich, F. Krueger, J. Rass, J.B. Park, V. Kueller, A. Knauer, T. Wernicke, M. Weyers, and M. Kneissl, J. Phys. D. Appl. Phys. **51**, 415101 (2018).

18) R. Dalmau, B. Moody, R. Schlesser, S. Mita, J. Xie, M. Feneberg, B. Neuschl, K. Thonke, R. Collazo, A. Rice, J. Tweedie, and Z. Sitar, J. Electrochem. Soc. **158**, H530 (2011).

19) S.G. Mueller, R.T. Bondokov, K.E. Morgan, G.A. Slack, S.B. Schujman, J. Grandusky, J.A. Smart, and L.J. Schowalter, Phys. Status Solidi A **206**, 1153 (2009).

20) Z. Bryan, I. Bryan, J. Xie, S. Mita, Z. Sitar, and R. Collazo, Appl. Phys. Lett. **106**, 1 (2015).

21) J.R. Grandusky, S.R. Gibb, M.C. Mendrick, C. Moe, M. Wraback, and L.J. Schowalter, Appl. Phys. Express **4**, 2 (2011).

22) T. Wunderer, C.L. Chua, J.E. Northrup, Z. Yang, N.M. Johnson, M. Kneissl, G.A. Garrett, H. Shen, M. Wraback, B. Moody, H.S. Craft, R. Schlesser, R.F. Dalmau, and Z. Sitar, Phys. Status Solidi C **9**, 822 (2012).

23) M. Martens, F. Mehnke, C. Kuhn, C. Reich, V. Kueller, A. Knauer, C. Netzel, C. Hartmann, J. Wollweber, J. Rass, T. Wernicke, M. Bickermann, M. Weyers, and M. Kneissl, IEEE Photonics Technol. Lett. **26**, 342 (2014).

24) Q. Guo, R. Kirste, S. Mita, J. Tweedie, P. Reddy, B. Moody, Y. Guan, S. Washiyama, A. Klump, Z. Sitar, and R. Collazo, J. Appl. Phys. **126**, 223101 (2019).

25) P. Fischer, J. Christen, M. Zacharias, V. Schwegler, C. Kirchner, and M. Kamp, Jpn. J. Appl. Phys. **39**, 2414 (2000).

26) M. Rossetti, T.M. Smeeton, W.S. Tan, M. Kauer, S.E. Hooper, J. Heffernan, H. Xiu, and C.J. Humphreys, Appl. Phys. Lett. **92**, 2006 (2008).

27) E.C. Young, F. Wu, A.E. Romanov, D.A. Haeger, S. Nakamura, S.P. Denbaars, D.A. Cohen, and J.S. Speck, Appl. Phys. Lett. **101**, 4 (2012).

28) A.M. Smirnov, E.C. Young, V.E. Bougrov, J.S. Speck, and A.E. Romanov, APL Mater. **4**, 016105 (2016).

29) S. Srinivasan, L. Geng, R. Liu, F.A. Ponce, Y. Narukawa, and S. Tanaka, Appl. Phys. Lett. **83**, 5187 (2003).

30) J. Moneta, M. Siekacz, E. Grzanka, T. Schulz, T. Markurt, M. Albrecht, and J. Smalc-Koziorowska, Appl. Phys. Lett. **113**, 031904 (2018).

31) R. Liu, J. Mei, S. Srinivasan, H. Omiya, F.A. Ponce, D. Cherns, Y. Narukawa, and T. Mukai, Jpn. J. Appl. Phys. **45**, L549 (2006).
32) B.S. Ooi, A.C. Bryce, C.D.W. Wilkinson, and J.H. Marsh, Appl. Phys. Lett. **64**, 598 (1994).
33) M. Avella, J. Jimńez, F. Pommereau, J.P. Landesman, and A. Rhallabi, Appl. Phys. Lett. **90**, 1 (2007).
34) S. Yamada, K. Takeda, M. Toguchi, H. Sakurai, T. Nakamura, J. Suda, T. Kachi, and T. Sato, Appl. Phys. Express **13**, 106505 (2020).
35) A. Kyrtsos, M. Matsubara, and E. Bellotti, Phys. Rev. B **93**, 1 (2016).
36) S. Limpijumnong and C. Van de Walle, Phys. Rev. B **69**, 035207 (2004).